



## Instability, Turbulence, and 3D Magnetic Reconnection in a Line-Tied, Zero Net Current Screw Pinch

Matthew I. Brookhart, Aaron Stemo, Amanda Zuberbier, Ellen Zweibel, and Cary B. Forest  
*University of Wisconsin-Madison, Madison, Wisconsin, USA*  
 (Received 12 December 2014; published 6 April 2015)

This Letter reports the first experimental investigation into a line-tied plasma with a reversed current profile. Discrete current sources create a cylindrical plasma equilibrium with an axial field and zero net current. Detailed magnetic measurements show that an internal  $m = 1$  mode with no external character grows exponentially. The nonlinear evolution of the mode drives 3D reconnection events that reorganize the plasma equilibrium. The plasma is turbulent and exhibits reconnection events on a range of scales. These data are consistent with recent simulations of coronal loops and the nanoflare coronal heating mechanism.

DOI: 10.1103/PhysRevLett.114.145001

PACS numbers: 52.72.+v, 52.35.Ra, 52.35.Vd

Current-driven magnetohydrodynamic (MHD) instabilities play an important role in many laboratory and astrophysical plasmas. The kink mode occurs when the plasma current twists magnetic field lines until they bend perpendicular to the field. In fusion experiments such as tokamaks, the external kink mode [1,2] can grow rapidly and disrupt plasma operation, while the internal kink mode [3] can drive magnetic reconnection in the sawtooth cycle [4,5]. Similarly, kink instabilities in coronal loops could contribute to the bursty magnetic energy release typical of solar flares [6].

In contrast to toroidal fusion devices, coronal loops are “line-tied” at the solar surface by the sharp transition from the magnetically dominated corona to the pressure dominated photosphere. Gold and Hoyle [7] proposed a solar flare model where magnetic field in a coronal loop is slowly twisted by motions in the Sun’s photosphere. Localized twisting motions in the photosphere generate a coaxial current structure with zero net current. In cylindrical coordinates,  $J_{\parallel} > 0$  at small  $r$  and  $J_{\parallel} < 0$  at large  $r$ .

Stability analysis for line-tied plasmas is more complicated than the analysis of periodic plasmas. An instability with a single wave number, appropriate for periodic plasmas, cannot satisfy line-tied boundary conditions. Instead, multiple modes with different wave numbers or three-dimensional simulations must be considered. Most numerical studies of the stability of the zero net current coronal loop use a straight, finite-length cylindrical approximation to the toroidal geometry of coronal loops. [8–14]. In these simulations, the zero net current coronal loop is unstable to an exponentially growing internal kink mode when the twist in the magnetic field ( $\Phi(r)$ ) is sufficiently large. Equivalently, the internal kink mode is unstable when the safety factor

$$q(r) = \frac{2\pi}{\Phi(r)} = \frac{2\pi r B_z}{L B_{\theta}} < q_{\text{crit}}, \quad (1)$$

where  $L$  is the length of the cylinder,  $r$  is the radial location, and  $B_{\theta}$  is the field generated by plasma current. The exact value of  $q_{\text{crit}}$  depends on the twist profile applied to the loop, but most zero net current equilibria are unstable at  $q_{\text{crit}} = 0.5\text{--}0.6$ .

While line-tied plasmas cannot form the current singularities present in toroidal geometries, early nonlinear simulations showed that the line-tied internal kink mode forms strong current sheets in the zero net current loop [10–13]. These current sheets then reconnect, dissipating up to 90% of the nonpotential magnetic energy in the loop. In recent higher resolution simulations, the kink-driven current sheet fragments into multiple reconnection sites and the system transitions into a self-organized state of magnetically driven turbulence [15,16].

To date, no experiments have created or studied the zero net current equilibrium. In tokamaks, experiments were performed attempting to create transient reversed current profiles using sources of noninductive current drive [17–20]. Plasma self-organization clamped the current profile to zero on the axis, preventing a reversed current equilibrium. Line-tied experiments have focused exclusively on plasmas with unidirectional current [21–26].

In this Letter we present the first experimental investigations into the stability of the zero net current equilibrium. Using a cylindrical, line-tied screw pinch experiment, the zero net current equilibrium is created for the first time in a laboratory. The equilibrium exhibits kinklike behavior, reconnection events, and turbulence. Comparisons to simulations are presented.

These experiments were performed on the Line Tied Reconnection Experiment, shown in Fig. 1, a modified version of the Rotating Wall Machine [27]. The device is a 2.08 m long, 20 cm diameter screw pinch. Eight external solenoids create a guide field  $B_z = 500\text{--}1300$  G with less than 2% ripple. A glass vacuum vessel minimizes the effect of the radial boundary condition on stability, allowing easy

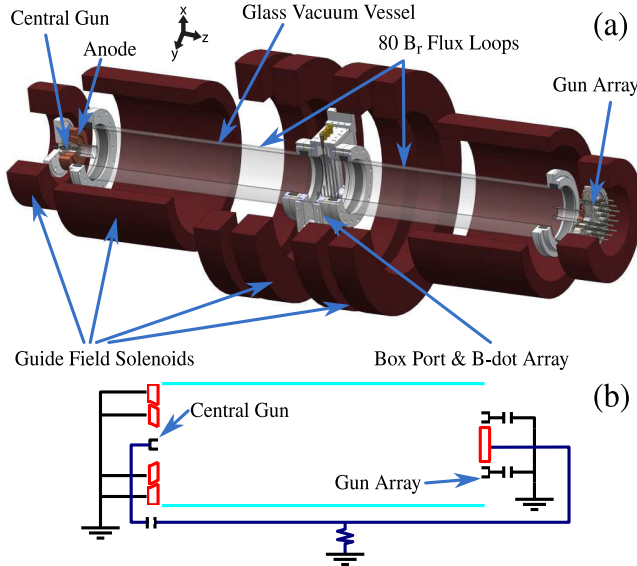


FIG. 1 (color online). The Line-tied Reconnection Experiment geometry. (a) A CAD model of the experiment with components highlighted. (b) A representation of the biasing circuit showing the independent supplies for each gun. The central gun floats with respect to the laboratory ground to prevent stray arc currents.

excitation of external kink modes. A plastic box port mounted at the axial midplane provides optical and probe access without disrupting the insulating boundary conditions.

Electrostatic guns [28] provide plasma density and current at both ends of the experiment. The azimuthal magnetic field is created by currents from the guns. Independently controlled power supplies bias each gun to create tailored current profiles. Thick copper anodes at the end of the experiment collect current and provide a rough current profile measurement. Because of the discrete nature of the plasma guns, the line-tying condition is firmly satisfied at the cathodes [21,22]. Hence, the central current is firmly tied at one end and the return current is tied at the other. In addition, the anodes have a resistive dissipation time of  $\tau \approx 200$  ms, indicating that magnetic fluctuations cannot penetrate the anodes on the time scales of a shot [24]. This property provides the line-tied boundary condition in the experiment. To create a zero-net current equilibrium, six guns produce a ring of negative plasma current at  $r = 3.63$  cm while a seventh gun, located on the other end of the experiment, provides positive current at the center of the device (see Fig. 5).

Eighty flux loops measure  $B_r$  at the insulating vacuum vessel and an array of 288 coils in a  $20 \text{ cm} \times 15 \text{ cm}$  cross section measures all three components of the magnetic field at the axial midplane of the experiment. High precision analog circuits integrate all magnetic signals before digitization. A Czerny-Turner spectrometer measures plasma density to be  $n_e = (0.5\text{--}3) \times 10^{20} \text{ m}^{-3}$  from the broadening of neutral hydrogen emission lines by the Stark effect. Plasma temperature is inferred from equilibrium

pressure reconstructions at  $T_e = 3\text{--}4$  eV, consistent with previous swept Langmuir probe measurements on the experiment [27]. The experiment has low  $\beta = 2\mu_0 p/B^2 = 1\%\text{--}3\%$ , similar to coronal values.

Alfvén wavelengths can propagate in the cylinder at frequencies less than the ion cyclotron frequency. Using  $\omega_A = \omega_{ci}$ , approximately 15 Alfvén wavelengths fit in the cylinder, providing ample space for Alfvénic turbulence. The Alfvén crossing time  $\tau_A = L/v_A \approx 10 \mu\text{s}$  is much shorter than the plasma discharge. The Lundquist numbers for these plasmas are  $S_{\parallel} = \mu_0 B_z a / \eta \sqrt{\rho \mu_0} \approx 120$  and  $S_{\perp} = \mu_0 B_{\theta} a / \eta \sqrt{\rho \mu_0} \approx 10$ . While experimental Lundquist numbers are much lower than coronal values, they are comparable to Lundquist numbers in published nonlinear simulations. The ion skin depth  $\delta_i/a = c/\omega_{pi} a \approx 0.4$ , where  $a = 5$  cm is the radial size of the plasma, indicating two fluid effects may be important.

An example plasma discharge is presented in Fig. 2. Part (a) plots current time traces from the central gun and the outer ring of six guns. The total current in the plasma, indicated by the light gray line, is close to zero. Example magnetic traces, in part (b), show large fluctuations inside the plasma but no fluctuations at the vacuum vessel. Time averaged spatial profiles of the magnetic field are charted in Fig. 3. A clear current reversal is present at  $r = 3$  cm.  $B_{\theta} = 0$  at  $r = 9$  cm; thus, Ampere’s law indicates a zero net current in the plasma. For this equilibrium, the safety factor  $q$  is minimal on the axis and  $q \rightarrow \infty$  at the large radius.

To illustrate the nature of the magnetic fluctuations in Fig. 2(b), we have explored the dynamics of the large events. An example is shown in Fig. 4(a). Large mode

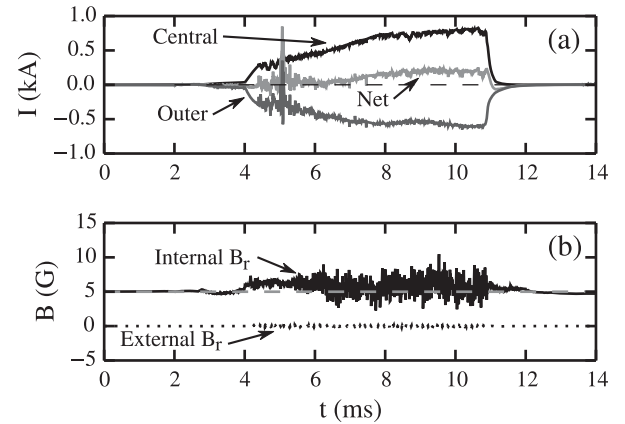


FIG. 2. An example discharge. (a) The current from the center gun, the outer guns, and the total plasma current. The plasma is created at  $t = 2$  ms and the biasing power supplies are engaged at  $t = 4$  ms. The plasma current is slowly increased over the course of the shot to prevent disruptions to the biasing power supplies. (b) The solid line is a trace from an internal magnetic probe located at  $z = 1.04$  m,  $r = 0.5$  cm; the fast fluctuations are due to internal plasma instabilities. The dashed line is a trace from an external probe located at  $z = 0.96$  m,  $r = 10$  cm; the internal instabilities do not appear on external diagnostics.

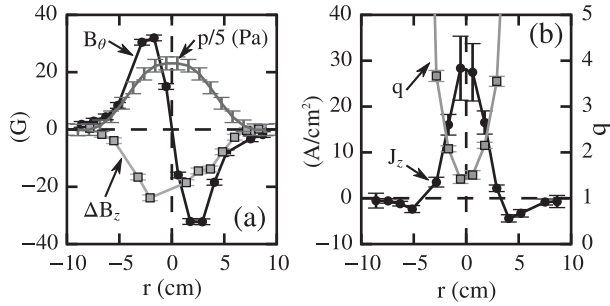


FIG. 3. An example zero-net Current equilibrium. (a) The measured  $\Delta B_z$ ,  $B_\theta$ , and pressure profiles. Note that  $B_\theta = 0$  at the edge of the vessel. The plasma is roughly isothermal, pressure gradients are due to decreased density at the plasma edge. (b) The current density with the reversal at 3 cm and the steep  $q$  profile.

activity occurs in the center of the plasma but the external magnetic array exhibits no  $m = 1$  activity above the noise floor. The mode exhibits exponential growth, but flattens from  $-8$  to  $-4 \mu\text{s}$ . This may be noise or nonlinear physics, so two exponentials are fit to find the growth rate. Both growth rates  $\gamma a/v_A = 0.027 \pm 0.006$  and  $\gamma a/v_A = 0.036 \pm 0.005$  are consistent with the linear growth rate of the ideal MHD internal kink mode in plasmas with zero-net-current equilibria [9,10,14].

Figure 5(a) presents a two-dimensional measurement of the plasma equilibrium [29]. While the plasma current is sourced from discrete guns, the current is azimuthally smoothed at the center of the experiment. The  $m = 1$  eigenstructure of the mode is clearly visible in Fig. 5(b). Additionally, a strong current sheet occurs at  $(x, y) = (-1, 4)$  cm. This spike in the current density, lasting for  $\approx 6 \mu\text{s}$ , is approximately 1.1–1.5 cm thick and  $6 \pm 1$  cm long at the axial location of the array. Less coherent, higher order structures are also routinely observed.

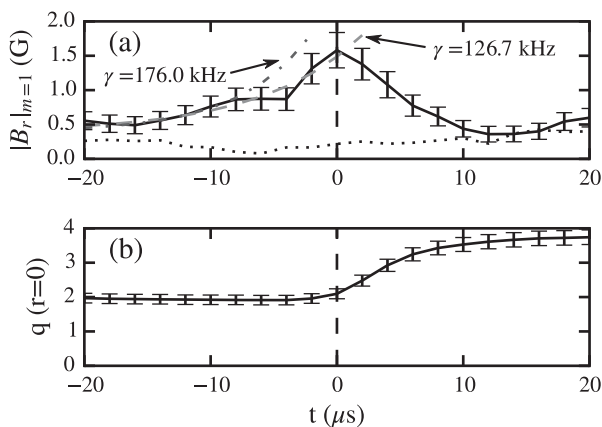


FIG. 4. A reconnection event. The solid black line in (a) is the  $m = 1$  component of  $B_r(r = 0)$ . Exponentials are fit for  $-20 < t < -8 \mu\text{s}$  and  $-20 < t < 0 \mu\text{s}$  to find mode growth rates. The  $m = 1$  component of the external magnetic array [dotted line in (a)] is below the noise floor. (b) shows the sharp increase in safety factor at the peak of the  $m = 1$  mode.

When the  $m = 1$  mode reaches its peak amplitude, the safety factor at the center of the plasma begins to rise, as shown in Fig. 4(b). This is consistent with the redistribution of current expected in a magnetic reconnection event. In total, approximately 40% of the nonpotential magnetic energy is dissipated by this event. Figure 6 graphs the current profile measured by (a) the internal array, and (b) the segmented anode, 20  $\mu\text{s}$  before and after the peak of the mode. There is a large drop in plasma current at the axis of the machine but very little change at the boundary of the experiment.

The growth rate, eigenstructure, and reconnection dynamics presented here are consistent with simulations of the ideal MHD internal kink mode in a zero net current plasma [10,12,13,15,16,30]. Unfortunately, this event does not match expected stability criteria:  $q = 1.9 \pm 0.2 \gg q_{\text{crit}} = 0.5\text{--}0.6$  [9,10,14,31]. Resistivity can destabilize the line-tied kink mode but the effect is not strong enough to explain these data [32]. Similarly, linear NIMROD [33] simulations (not shown) indicate that the Hall effect can destabilize the kink by 5%–10%, and is also not enough to

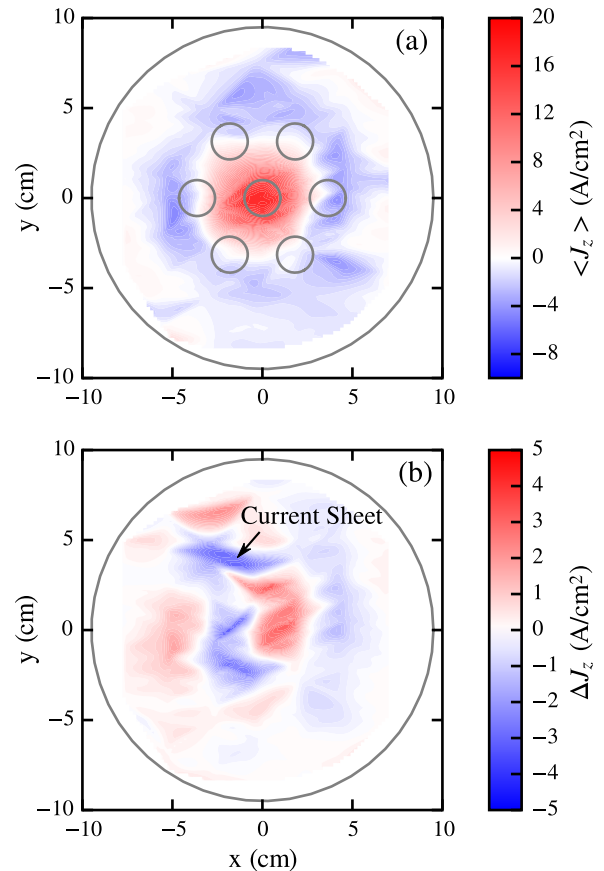


FIG. 5 (color online). (a) The time-averaged current density. While the plasma current is sourced at discrete locations, currents have merged azimuthally prior to reaching the probe array. (b) The current perturbation at the peak of the  $m = 1$  activity. The  $m = 1$  perturbation is clear, as is evidence for a current sheet at  $(x, y) = (-1, 4)$  cm.

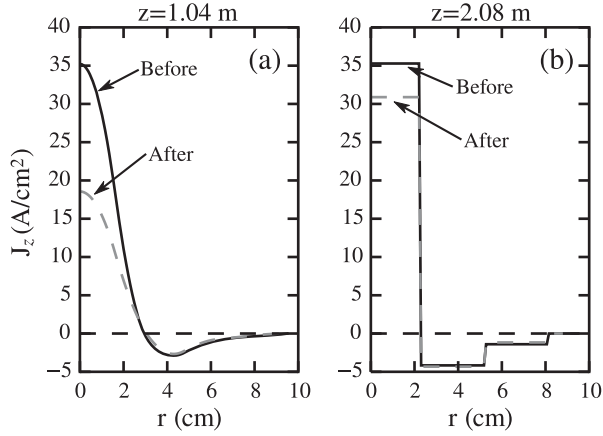


FIG. 6. The current profile 20  $\mu$ s before (black) and after (gray) the crash shown in Fig. 4. (a) shows a fit to the internal magnetic data measured 1.04 m from the guns. Notice how the central current density decreases by a factor of 2. Error on the fit is  $\pm 2$  A/cm<sup>2</sup>. (b) shows the current profile measured at the anode (2.08 m from the guns) of the experiment. The drop in the central current is much lower.

explain the data. An analysis of 2078 reconnection events in the data shows no critical instability conditions. These events display a wide range of safety factors ( $q = 1.2$ – $3$ ), current sheet sizes ( $L = < 1$ – $6$  cm), and energy dissipation (10%–80%).

Instead of an internal kink mode, these events may be self-organized turbulent structures. An aggregated power spectrum in Fig. 7 shows a clear  $f^{-5/3}$  spectrum. Measurements of the wave number spectrum are consistent with  $k_{\perp}^{-5/3}$  (not shown), but have large uncertainty due to limited spatial resolution. This spectrum indicates a turbulent cascade to some dissipation scale. This fluctuation pi

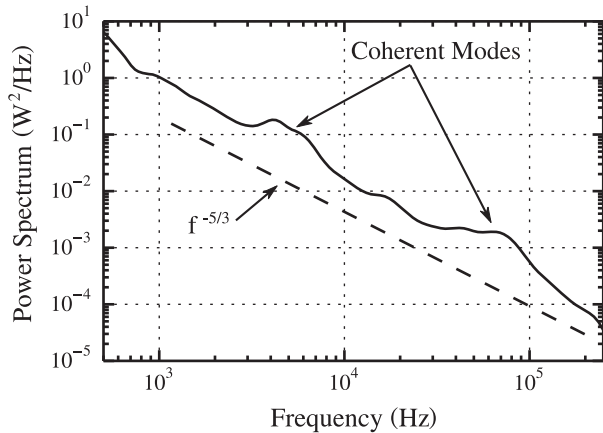


FIG. 7. The power spectrum of the magnetic field calculated with the Morlet wavelet. The dashed line indicates  $f^{-5/3}$ , matching the data. Additionally, two coherent modes rise above the background spectrum. The lower frequency mode is the plasma rotation due to  $\vec{E} \times \vec{B}$  drifts. The higher frequency mode might be drift-Alfvén activity and is beyond the scope of this work.

twb .45wspectrum, combined with the large spread in reconnection dynamics we observe, indicates that the plasma is in a fully turbulent state. The experiment exhibits turbulence very early in the plasma discharge [as shown in Figure 2(b)] which may be seeded by fluctuations in the guns. Interestingly, turbulence seems to relax the equilibrium, preventing the equilibrium from reaching linear instability.

This picture of turbulent relaxation is qualitatively consistent with recent simulations by Rappazzo *et al.* [30]. In those simulations, magnetically driven turbulence stochastically dissipates magnetic energy at a variety of scales. These turbulent reconnection events relax the coronal loop, raising the safety factor and stabilizing the kink mode for the duration of the simulation. These turbulent reconnection events heat the corona, similar to the Parker model of nanoflares [34,35].

These results are the first demonstration of the zero-net-current equilibrium in the laboratory. These data are also the first unambiguous demonstration of internal modes driving three-dimensional reconnection in a line-tied plasma. Bergerson *et al.* [21] presented evidence of the internal kink mode in a line-tied screw pinch with a monotonic current profile, but no internal diagnostics were available for those experiments. The lack of internal data left some ambiguity on the internal and external nature of the observed mode [23].

Many reconnection events in this plasma are clearly turbulent structures. At this point it is difficult to determine if the larger  $m = 1$  modes observed are the result of an internal kink with a modified stability criterion or if they are also self-organized turbulent structures. Turbulent reconnection events likely heat the plasma, but current temperature diagnostics are limited by sensitivity. While the experimental boundary conditions match the corona, the current drive in the experiment may not react to reconnection events the same way that the corona does. This may change the statistical nature of turbulence in the experiment. Future work will investigate these turbulent statistics to understand mode stability, nonlinear evolution, and plasma heating. Current experimental capabilities do not measure the three-dimensional topology of reconnection events and turbulence. Additional probes at other  $z$  locations will allow measurements of field lines and the three-dimensional structure of reconnection events.

This work is supported by U.S. Department of Energy Grant No. DE-SC0008708 and by National Science Foundation Grant No. 0903900. We wish to thank Hanto Ji, Jon Jara-Almonte, John Sarff, and Darren Craig for assistance in the design of the internal probe array and analog integrators. We also wish to acknowledge the many individuals of the University of Wisconsin Plasma Physics Group and the Center for Magnetic Self-Organization (CMSO) who have provided their guidance, support, and time to our work.

- [1] V. D. Shafranov, *At. Energ.* **1**, 709 (1956), *Sov. J. At. Energy* **1**, 38 (1956).
- [2] M. Kruskal and J. L. Tuck, *Proc. R. Soc. A* **245**, 222 (1958).
- [3] V. D. Shafranov, *Zh. Tekh. Fiz.* **40**, 241 (1970). [*Tech. Phys.* **15**, 175 (1970)].
- [4] M. N. Rosenbluth, R. Y. Dagazian, and P. H. Rutherford, *Phys. Fluids* **16**, 1894 (1973).
- [5] B. B. Kadomtsev, *Fiz. Plazmy* **1**, 710 (1975). [*Sov. J. Plasma Phys.* **1**, 389 (1975)].
- [6] K. Shibata and T. Magara, *Living Rev. Solar Phys.* **8**, 57 (2011).
- [7] T. Gold and F. Hoyle, *Mon. Not. R. Astron. Soc.* **120**, 89 (1960).
- [8] P. K. Browning and A. W. Hood, *Sol. Phys.* **124**, 271 (1989).
- [9] Z. Mikic, D. D. Schnack, and G. van Hoven, *Astrophys. J.* **361**, 690 (1990).
- [10] R. Lionello, D. D. Schnack, G. Einaudi, and M. Velli, *Phys. Plasmas* **5**, 3722 (1998).
- [11] R. Lionello, M. Velli, G. Einaudi, and Z. Mikić, *Astrophys. J.* **494**, 840 (1998).
- [12] C. L. Gerrard, T. D. Arber, A. W. Hood, and R. A. M. Van der Linden, *Astron. Astrophys.* **373**, 1089 (2001).
- [13] C. L. Gerrard, T. D. Arber, and A. W. Hood, *Astron. Astrophys.* **387**, 687 (2002).
- [14] Y.-M. Huang, E. G. Zweibel, and C. R. Sovinec, *Phys. Plasmas* **13**, 092102 (2006).
- [15] P. K. Browning, C. Gerrard, A. W. Hood, R. Kevis, and R. A. M. V. D. Linden, *Astron. Astrophys.* **485**, 837 (2008).
- [16] A. W. Hood, P. K. Browning, and R. A. M. V. D. Linden, *Astron. Astrophys.* **506**, 913 (2009).
- [17] T. Fujita, T. Oikawa, T. Suzuki, S. Ide, Y. Sakamoto, Y. Koide, T. Hatae, O. Naito, A. Isayama, N. Hayashi, and H. Shirai, *Phys. Rev. Lett.* **87**, 245001 (2001).
- [18] N. C. Hawkes, B. C. Stratton, T. Tala, C. D. Challis, G. Conway, R. DeAngelis, C. Giroud, J. Hobirk, E. Joffrin, P. Lomas, P. Lotte, J. Mailloux, D. Mazon, E. Rachlew, S. Reyes-Cortes, E. Solano, and K. D. Zastrow, *Phys. Rev. Lett.* **87**, 115001 (2001).
- [19] D. Merkl, J. Hobirk, P. McCarthy, L. Giannone, O. Gruber, V. Igochine, M. Maraschek, G. Pereverzev, W. Schneider, A. Sips, E. Strumberger, and ASDEX Upgrade Team, in *Proc. 30th EPS Conf. on Control. Fusion and Plasma Physics* (Max-Planck Institute for Plasma Physics, St. Petersburg, 2003), p. 1.134.
- [20] R. J. Jayakumar, M. Austin, C. M. Greenfield, N. C. Hawkes, J. E. Kinsey, L. L. Lao, P. B. Parks, E. R. Solano, and T. S. Taylor, *Nucl. Fusion* **48**, 015004 (2008).
- [21] W. F. Bergerson, C. B. Forest, G. Fiksel, D. A. Hannum, R. Kendrick, J. S. Sarff, and S. Stambler, *Phys. Rev. Lett.* **96**, 015004 (2006).
- [22] T. P. Intrator, X. Sun, G. Lapenta, L. Dorf, and I. Furno, *Nat. Phys.* **5**, 521 (2009).
- [23] E. Oz, C. E. Myers, M. Yamada, H. Ji, R. M. Kulsrud, and J. Xie, *Phys. Plasmas* **18**, 102107 (2011).
- [24] C. Paz-Soldan, M. I. Brookhart, A. J. Clinch, D. A. Hannum, and C. B. Forest, *Phys. Plasmas* **18**, 052114 (2011).
- [25] C. Paz-Soldan, M. I. Brookhart, A. T. Eckhart, D. A. Hannum, C. C. Hegna, J. S. Sarff, and C. B. Forest, *Phys. Rev. Lett.* **107**, 245001 (2011).
- [26] W. Gekelman, E. Lawrence, and B. Van Compernelle, *Astrophys. J.* **753**, 131 (2012).
- [27] C. Paz-Soldan, W. F. Bergerson, M. I. Brookhart, D. A. Hannum, R. Kendrick, G. Fiksel, and C. B. Forest, *Rev. Sci. Instrum.* **81**, 123503 (2010).
- [28] G. Fiksel, A. F. Almagri, D. Craig, M. Iida, S. C. Prager, and J. S. Sarff, *Plasma Sources Sci. Technol.* **5**, 78 (1996).
- [29] See Supplemental Material at <http://link.aps.org/supplemental/10.1103/PhysRevLett.114.145001> for a video of the plasma evolution.
- [30] A. F. Rappazzo, M. Velli, and G. Einaudi, *Astrophys. J.* **771**, 76 (2013).
- [31] H. Baty, *Astron. Astrophys.* **367**, 321 (2001).
- [32] G. L. Delzanno, E. G. Evstatiev, and J. M. Finn, *Phys. Plasmas* **14**, 070702 (2007).
- [33] C. R. Sovinec, *J. Comput. Phys.* **195**, 355 (2004).
- [34] E. N. Parker, *Astrophys. J.* **174**, 499 (1972).
- [35] E. N. Parker, *Astrophys. J.* **330**, 474 (1988).